Journal of Materials Chemistry B

RSC Publishing

PAPER

View Article Online
View Journal | View Issue

Cite this: J. Mater. Chem. B, 2013, 1, 685

Antibacterial properties and bioactivity of HACC- and HACC–Zein-modified mesoporous bioactive glass scaffolds†

Panyu Zhou,‡[a] Yan Xia,‡[a] Jing Wang,‡[b] Chong Liang,‡[c] Long Yu,[d] Wei Tang,[b] Shen Gu*[e] and Shuogui Xu*[abcde]

Infection and its complications are one of the greatest threats to the health of orthopedic patients. Mesoporous bioglass (MBG) scaffolds are characterized by well-ordered, three-dimensional, nanometer-sized mesoporous structures, which facilitate the adhesion of hydroxyapatite and the loading of drugs. MBG has been widely used as a new-generation biomaterial in bone tissue engineering. However, MBG is very brittle and lacks antibacterial activity. This limits its applications in the treatment of bone defects, especially large bone defects complicated by infection. In order to dispel these disadvantages, a novel hydroxypropyltrimethyl ammonium chloride chitosan (HACC) and a class of prolamine proteins found in maize, Zeins, were here used to modify the traditional MBG scaffolds. Two new types of scaffold, MBG–HACC scaffolds and MBG–HACC–Zein scaffolds, were made. Transmission electron microscopy (TEM), small angle X-ray diffraction (SAXRD), and Barrett–Joyner–Halenda (BJH) were used to analyze the surface properties of these MBG scaffolds. Fourier transform infrared spectroscopy (FTIR), X-ray diffraction (XRD), scanning electron microscopy (SEM), mechanical experiments, and synchrotron radiation microcomputer tomography (SRμCT) were used to compare the features of the traditional and modified scaffolds and to analyze the mineralization of the scaffold after being soaked in simulated body fluid (SBF). Confocal laser scanning microscopy (CLSM) was used to compare the antibacterial properties and biocompatibility of the scaffolds at various points in time. The current study demonstrates that all these prepared MBG scaffolds possessed well-ordered, three-dimensional, nanometer-sized mesoporous structures and that HACC–Zein-modified MBG scaffolds are characterized by strong bioactivity and by effective, prolonged antibacterial activity. Finally, biocompatibility was demonstrated by studying the *in vitro* proliferation and viability of human mesenchymal stem cells (hMSCs).

Received 11th September 2012
Accepted 20th November 2012

DOI: 10.1039/c2tb00102k

www.rsc.org/MaterialsB

1 Introduction

The development of synthetic scaffolds suitable for use in bone regeneration and other applications poses a significant challenge in the regenerative medical field. These scaffolds must have specific pore architectures, mechanical strengths, bioactivity levels, and degradation properties and must deliver drugs in a controllable way.[1] Currently, only a few synthetic scaffolds have all of these properties. There are no scaffolds that can be used to repair large bone defects. The development of new, porous, 3D scaffolds for bone regeneration has drawn the attention of many researchers.[2–4] Yan *et al.* prepared the first multicomponent mesoporous bioactive glass (MBG) in 2004 using a SiO_2–CaO–P_2O_5 system.[5] This was the initial work of the new biomaterials subfield, and many applications for the bioglasses discovered by Hench *et al.* in 1969 have been found.[6] MBG differs from non-mesoporous bioactive glass (NBG) in that it possesses a significantly greater specific surface area and a greater total nano-pore volume. These characteristics render it

[a]Changhai Hospital, Department of Orthopedics, the Second Military Medical University, 168 Changhai Road, Shanghai 200433, China. E-mail: summer520m@163.com; Fax: +86-21-55226616; Tel: +86-21-31161687

[b]Engineering Research Center for Biomedical Materials of Ministry of Education, East China University of Science and Technology, 130 Meilong Road, Shanghai 200237, China. E-mail: wjbiomat@yahoo.com.cn; Fax: +86-21-64253631; Tel: +86-21-64251358

[c]The 81 Hospital of People's Liberation Army of China, Department of Neurosurgery, 34 Taiping Road, Nanjing 210002, China. E-mail: liangchong1984@163.com; Fax: +86-21-55226616; Tel: +86-25-80864053

[d]Xijing Hospital, Institute of Orthopedics, the Fourth Military Medical University, 15 Changle Road, Xi'an 710033, China. E-mail: xijingguke@163.com; Fax: +86-29-3375292; Tel: +86-29-3375291

[e]Academy of Nursing, the Second Military Medical University, 800 Xiangyin Road, Shanghai 200433, China. E-mail: Bonexu@yahoo.cn; Fax: +86-21-81871504; Tel: +86-21-81871503

† Electronic supplementary information (ESI) available. See DOI: 10.1039/c2tb00102k

‡ These authors contributed equally to this work.

suitable for certain applications, as evidenced by its superior apatite-mineralization ability and biocompatibility.[7,8] Ordered mesoporous bioactive glasses (MBG) have recently shown promise as bone reconstruction materials.[5,9,10] These materials can be loaded with osteogenic agents and drugs, which promote the growth of new bone.[11,12] Like other inorganic scaffolds, however, MBG scaffolds are very brittle. Their low mechanical strength makes them unsuitable for some applications. They also lack inherent antibacterial activity.[13]

Infection is one of the most serious and devastating complications faced by the millions of patients who undergo orthopedic procedures annually. It increases the incidence of osteomyelitis, bone necrosis, septicemia, and loss of mobility in the dead zone. These conditions can impose a huge economic burden on society.[14–16] Preventive measures include both systemic and local antibiotics, and many of these measures have been shown to be somewhat effective in the prevention of infection in both experimental and clinical settings.[17,18] However, overuse of antibiotics has caused the emergence of antibiotic-resistant bacteria.[19,20] For this reason, more effective antimicrobial agents suitable for use in prophylaxis and treatment must be investigated, especially agents effective against antibiotic-resistant organisms.

The biopolymer chitosan is non-toxic and naturally biodegradable. It is obtained through the deacetylation of chitin and it has been shown to have intrinsic activity against many different kinds of bacteria, filamentous fungi, and yeast.[21–24] Recent studies have demonstrated that chitosan is strongly biocompatible with bone cells, to the point where it can be used as a scaffold for bone tissue engineering.[25,26] However, bone tissue engineering applications benefit from the use of materials with antibiotic properties, and the antibiotic activity of chitosan is limited by its poor solubility in water.[27] In one previous study, we successfully synthesized a new water-soluble chitosan derivative (hydroxypropyltrimethyl ammonium chloride chitosan, HACC). We found that the antibacterial activity and biocompatibility of HACC could be balanced by varying the DS (degree of substitution) of the quaternary ammonium.[28] Tan *et al.* and Wu *et al.* found HACC modified-scaffolds showed good antibacterial activity within 24 h.[29,30] To the best of our knowledge, few investigations have focused on the antibacterial activity of HACC after 24 h.

Zein is one of the major starch storage proteins in corn. It is rich in non-polar amino acid residues, which make it insoluble in water, but it is soluble in aqueous solutions of ethanol (60–95%).[31–34] Zein shows strong hydrophobicity, forming films that act as a barrier to moisture and oxygen.[35] It has been used extensively in adhesives, fibers, chewing-gum, coatings for food products, biodegradable plastics, drug delivery matrices, and cosmetic powders and in the preparation of microencapsulated pesticides.[36,37] In this study, HACC and Zein were used in combination. They would adhere to the surfaces of the MBG scaffolds and improve their mechanical properties. In this way, the scaffolds acquired antibacterial activity because of HACC and showed a long-lasting antibacterial effect attributable to the film-forming properties of Zein.

2 Materials and methods

2.1 Materials

HACC was prepared by combining chitosan with glycidyl trimethylammonium chloride (GTMAC), as previously reported.[28] Chitosan (CS) with a molecular weight of 2.0×10^5 and an *N*-deacetylation rate of 95.0% was purchased from Zhejiang Yuhuan Ocean Biochemistry Co., Ltd., China.

2.2 Preparation and characterization of HACC- and HACC–Zein-modified MBG scaffolds

Porous mesoporous-bioglass (MBG) scaffolds were prepared using P123 (EO_{20}–PO_{70}–EO_{20}) and polyurethane sponges, as described previously.[38] Typically, 4.0 g of P123 ($M_w = 5800$, Aldrich), 1.0 g of 0.5 M HCl, 1.4 g of $Ca(NO_3)_2 \cdot 4H_2O$, 0.73 g of triethyl phosphate (TEP, 99.8%) and 6.7 g of tetraethyl orthosilicate (TEOS, 98%) were dissolved in 60 g of ethanol (Si/Ca/P = 80 : 15 : 5, molar ratio). This mixture was stirred at room temperature for 1 day. The polyurethane sponges (20 ppi) were immersed in this solution, allowed to soak for 10 min, and transferred to a Petri dish. Excess solution was removed and then the sponges were allowed to air-dry at room temperature for 12 h. The sponges were re-soaked and re-dried several times. When the samples were completely dry, they were calcined at 600 °C for 5 h, producing the MBG scaffolds. The mesopore-channel structures of the scaffolds were characterized by transmission electron microscopy (TEM), Fourier-transform infrared spectroscopy (FT-IR), small-angle X-ray diffraction (SAXRD), and Brunauer–Emmett–Teller (BET). The calcined scaffolds were immersed in HACC water solutions (8.0% w/v) for 3 min and centrifuged at 1000 rpm to remove any excess HACC solution. The scaffolds were air-dried in a fume hood for 1 day and then dried at 40 °C for 1 day. The HACC-modified scaffolds are referred to as MBG–HACC throughout this text.

MBG–HACC scaffolds were immersed in Zein ethanol solutions (8%) to prepare HACC–Zein modified MBG scaffolds (MBG–HACC–Zein). The following procedure was the same as the one used for the preparation of MBG–HACC. The amounts of HACC and Zein in the modified MBG were confirmed by thermal gravimetric analysis (TGA).

Scanning electron microscopy was used to examine the pore structure and surface microstructure of the pore walls of the scaffolds (SEM, Quanta 250, FEI). FTIR was used to examine chemical composition. The compression tests were performed on a universal material testing machine (Instron 5567, Instron Corp., U.S.), equipped with a Model 2519-104 force transducer at a crosshead speed of 0.5 mm min^{-1}. SRμCT measurements were performed at beamline BL13W of SSRF (Shanghai, China). The tests involved a monochromatic beam with an energy of 30 keV and a sample-to-detector distance of 1.5 m. A 4000 × 2500 CCD detector with a 6 mm pixel size was used to record images. One thousand two hundred projections within an angular range of 180° were taken. The total exposure time per projection was 8 s. The 3D structure was reconstructed using a filtered back-projection algorithm. These images were redigitized with an 8-bit data format, which was proportional to the measured attenuation

coefficients of the voxels. VG Studio MAX 2.0 software (Volume Graphics, Heidelberg, Germany) was used for the visualization of the tomographic data. Scaffolds with dimensions of 10 × 10 × 10 mm were then subjected to mechanical tests.

2.3 *In vitro* bioactivity tests

The scaffolds were placed in polyethylene containers and soaked in 50 ml of filtered simulated body fluid (SBF). The containers were stirred at 100 rpm and maintained at a temperature of 37 °C for 2 days. The evolution of their surfaces was analyzed by FTIR spectroscopy, XRD, and SEM.

2.4 Formation of bacterial biofilms

The ability of each strain to form biofilms on the scaffolds was analyzed using a method described in a previous report.[9] The inocula were prepared by adjusting the concentration of an overnight bacterial broth culture to 1×10^6 CFUs ml^{-1} in Tryptic Soy Broth medium (TSB) as described by McFarland. The scaffolds were placed in a 48-well plate and 1 ml of the suspension was added (Costar3548, U.S.). This mixture was incubated at 37 °C with agitation at 100 rpm for 72 h. At 24 h and again at 72 h, the scaffolds were removed with sterile forceps and placed in fresh 24-well plates. They were then gently washed three times with PBS. The discs were then placed in a new 48-well plate and stained with 0.5 ml combination dye (LIVE/DEAD Baclight bacteria viability kits, Molecular Probes, L13152). They were then analyzed with a confocal laser scanning microscope (Nikon A1R, Japan). The viable cells appeared green and the nonviable bacteria were stained fluorescent red because of their damaged membranes. The biofilm images were analyzed using Nikon confocal software. The images were taken at random positions on the surfaces of the scaffolds.

2.5 Quantitative measurements of bactericidal properties

Total bacterial growth was used as a negative indicator of scaffold bactericidal properties.[39] First, bacteria at a concentration of 1×10^6 CFUs ml^{-1} were incubated with the three scaffolds for 24 h to allow biofilms to form. The bacteria retained on the substrates were dislodged by mild ultrasonication and rapid vortex mixing. Total bacterial population was determined using serial dilution of 0.1 ml samples of the bacterial suspension. The number of total bacteria was calculated and normalized to that of the MBG control suspension.

2.6 Cell culture

Human mesenchymal stem cells (hMSCs) were donated to this project by the Shanghai Ninth People's Hospital (Shanghai, China). They were propagated in alpha-modified minimum essential medium (α-MEM) supplemented with 10% (v/v) fetal bovine serum (FBS). The cells were kept in a humidified incubator at 37 °C and 5% CO_2. The medium was replaced every 3 days.

2.7 Viability of cells cultured on scaffolds

The 6 × 6 × 6 mm scaffolds were sterilized with gamma radiation (15 kGy). All scaffolds were soaked in the α-MEM solution for 24 h. Fifty microliters of passage 3 cells in suspension (5×10^4 cells per well) were seeded onto each scaffold. After 2 h, 950 μl of culture medium was added into each well. The cells and scaffold constructs were incubated for 24 h at 37 °C in a humidified incubator at 5% CO_2.

Cell viability was evaluated using a live/dead assay kit in accordance with the manufacturer's instructions (Biotium, U.S.). The relative number of live cells was calculated as the number of live cells/(the number of live cells + the number of dead cells). The cells and scaffold constructs were first washed twice with PBS and then incubated in standard working solution at room temperature for 45 min. The constructs were washed twice with PBS and then observed using fluorescence microscopy (Nikon, Japan).

2.8 Cell proliferation

The hMSCs were cultured for 7 days, and their proliferation was assessed on days 1, 4, and 7 using a 3-(4,5-dimethylthiazol-2-yl)-2,5-diphenyltetrazolium bromide (MTT) assay. Briefly, the scaffolds were placed into a 48-well plate and seeded with 1 ml of cell suspension at a cell density of 5×10^3 viable cells. Another 48-well plate containing 1 ml of the a-MEM culture medium and the scaffolds served as a parallel control. At the prescribed point in time, 0.1 ml of the MTT solution was added and the specimens were incubated at 37 °C to form formazan. The formazan was then dissolved using DMSO. The optical density (OD) was measured at 570 nm using an automated plate reader (Synergy HT multidetection microplate). The mean absorbance obtained from the medium-control well was calculated using test absorbance values.

2.9 Statistical analysis

Experiments were performed 4 times per biological replicate. The results are expressed as means ± standard deviations. Compressive strength was assessed using one-way analysis of variance (ANOVA). The two means were analyzed using Tukey's test. $P < 0.05$ was considered significant.

3 Results

3.1 Characterization of MBG

The TEM images of MBG are illustrated in Fig. 1. As shown in Fig. 1a, MBG exhibited ordered pore arrays. Fig. 1b presents the same scenario at higher magnification. In this image, we

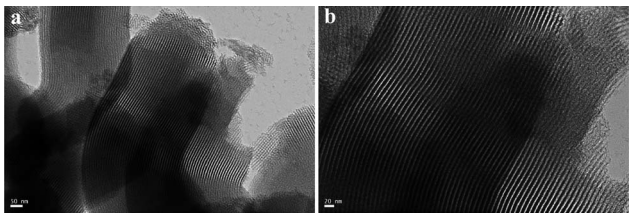

Fig. 1 TEM images of the prepared MBG scaffolds showing their highly ordered mesopore-channel structure.

observed a uniform and homogeneously distributed 2D-hexagonal channel structure of approximately 5 nm in size.

The SAXRD patterns of MBG are shown in Fig. 2. The SAXRD pattern of MBG shows three diffraction peaks in the small-angle regime ($2\theta = 1.13°$, 1.95°, and 2.30°). These peaks were indexed to the (100), (110), and (200) diffraction peaks, indicating that MBG has a uniform homogeneously distributed 2D-hexagonal pore structure (space group: *p6mm*). This is consistent with TEM observations.

The nitrogen adsorption–desorption isotherm of MBG is type IV. It has capillary condensation behavior characteristic of gas in mesopores (Fig. 3). The inset of Fig. 3 shows the pore size distribution curve as calculated from the adsorption branch by the Barrett–Joyner–Halenda (BJH) model. For MBG, a high BET-specific surface area of 727.8 m^2 g^{-1} is found. A total pore volume of 0.51 cm^3 g^{-1} was obtained. A narrow peak appeared in the BJH pore-size distribution curve, centered at 6.18 nm. This indicated that the mesopores were uniform in size. This is consistent with the results of SAXRD and TEM analysis.

3.2 Characterization of different scaffolds

3.2.1 TGA. According to the TGA data, in the HACC-modified MBG scaffolds, HACC accounted for 15.8% of the total mass. In the HACC–Zein- modified MBG scaffolds, Zein accounted for 21.4% (Fig. 4).

3.2.2 FT-IR. The functionalized MBGs were investigated by FT-IR spectroscopy analysis. The FT-IR spectra for (A) Zein, (B) MBG, (C) HACC, (D) MBG–HACC, and (E) MBG–HACC–Zein before and (F) after soaking in SBF for 4 weeks are shown in Fig. 5. Unlike those of MBG, the spectra for the group containing HACC showed characteristic absorption peaks for C–H of the trimethylammonium group at 1480 cm^{-1}. The absorption at 1587 cm^{-1}, attributed to the vibration of N–H bonds, was also detected. These findings demonstrate that HACC had been grafted onto the surfaces of MBG–HACC and MBG–HACC–Zein. The absorption bands at around 3400 cm^{-1} were attributed to the vibration of Zein bonds and were clearly visible. This confirmed that Zein groups had also been successfully grafted onto the surface of MBG–HACC–Zein.

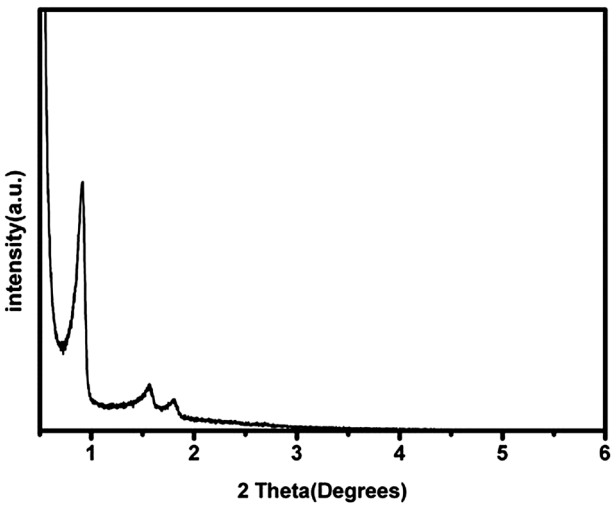

Fig. 2 Small-angle XRD pattern of MBG scaffolds. Images indicate that MBG has 2D-hexagonal pore structures.

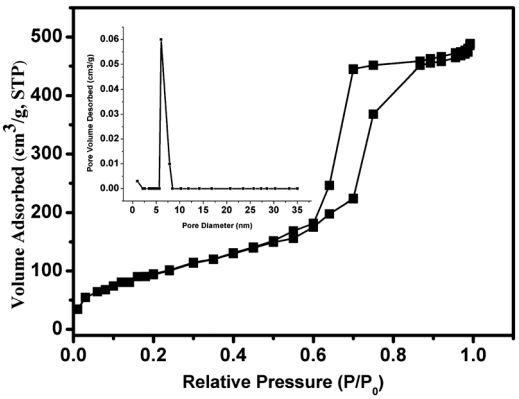

Fig. 3 Nitrogen adsorption–desorption isotherm and distribution of mesopores by size distribution (inset) for MBG scaffolds.

In vitro bioactivity tests of MBG–HACC–Zein began with soaking the scaffolds in SBF. The formation of an apatite-like phase was evaluated using FTIR spectroscopy, as established by Warren *et al.*[40] MBG–HACC–Zein FTIR spectra were collected before and after 4 weeks of soaking in SBF. They showed the bulk formation of a new apatite phase (Fig. 5F). These spectra showed absorption bands corresponding to the chemical functional groups of the glass component. A peak consistent with the Si–O–Si asymmetric stretching mode was observed at 1091 cm^{-1} and a vibration attributable to the symmetric Si–O–Si stretching and vibration modes of the silica ring structures was observed at 800 cm^{-1}. The peak for the Si–O–Si bending mode was observed at 490 cm^{-1}. The low-intensity signal at 560 cm^{-1} detected in spectra produced by MBG–HACC–Zein pieces before soaking was attributed to the phosphate groups in an amorphous environment. Finally, the double peak at 570 and 600 cm^{-1} in spectra produced by MBG–HACC–Zein after 4 weeks in SBF was attributed to the P–O bending mode related to the presence of crystalline phosphate in the glasses, which appeared after the reaction with the SBF.

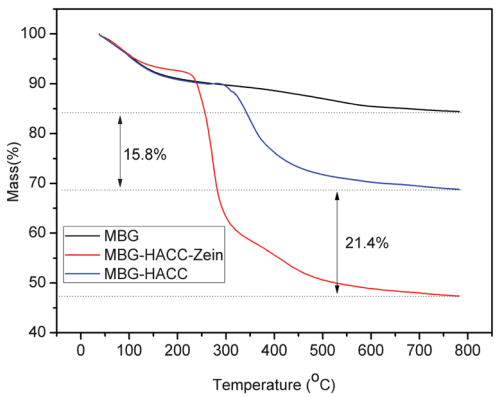

Fig. 4 TGA of MBG, MBG–HACC and MBG–HACC–Zein scaffolds.

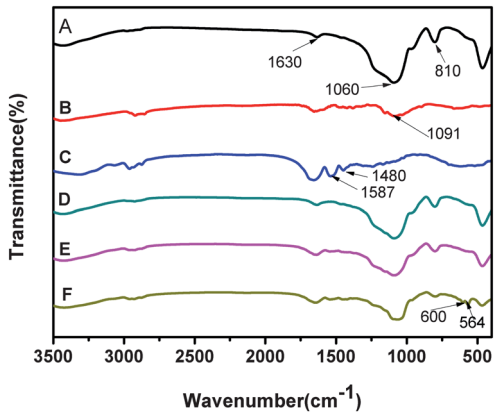

Fig. 5 FT-IR spectra of (A) Zein, (B) MBG, (C) HACC, (D) MBG–HACC, and (E) MBG–HACC–Zein before and (F) after soaking in SBF for 4 weeks.

3.2.3 XRD. Fig. 6 shows the X-ray (XRD) diffraction of (A) HACC, (B) MBG, (C) Zein, (D) MBG–HACC, and (E) MBG–HACC–Zein before and (F) after soaking in SBF for 4 weeks. A broad peak around $2\theta = 23^\circ$ was observed in the HACC spectrum but not in the unmodified MBG spectrum. This demonstrates that HACC groups have been grafted onto the surface of MBG–HACC and MBG–HACC–Zein. Similarly, a peak around $2\theta = 23^\circ$, attributed to Zein bonds, was clearly visible. This confirms that the Zein groups have also been successfully grafted onto the surface of the MBG–HACC–Zein complex. After immersion in the SBF solution, the samples of MBG–HACC–Zein showed peaks at 25.88°, 31.77°, and 49.47°, showing the typical (002), (211), and (213) diffractions for HA, indicating precipitation of HA on the MBG–HACC–Zein scaffold after immersion in SBF.

3.2.4 SEM. As shown in Fig. 7a, e, and i, the general morphology of each scaffold was observable, with MBG, MBG–HACC, and MBG–HACC–Zein scaffolds showing increasing degrees of surface roughness. Some of the pore walls of the MBG scaffold were ruptured, and the pore walls of the MBG–HACC and MBG–HACC–Zein scaffolds remained intact, indicating that HACC and Zein could reduce the brittleness of MBG.

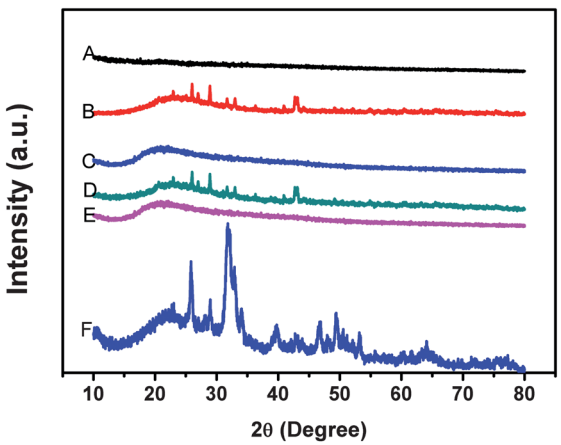

Fig. 6 X-ray diffraction of (A) HACC, (B) MBG, (C) Zein, (D) MBG–HACC, (E) MBG–HACC–Zein before and (F) after soaking in SBF for 4 weeks.

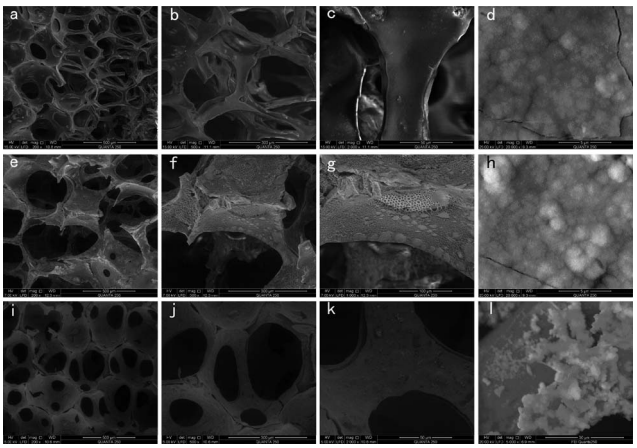

Fig. 7 Surface microstructure of (a–c) MBG, (e–g) MBG–HACC, and (i–k) MBG–HACC–Zein scaffolds at different magnification levels. SEM of (d) MBG, (h) MBG–HACC, and (l) MBG–HACC–Zein scaffolds after soaking in SBF for 4 weeks are also shown.

As shown in Fig. 7b, f, and j, the general morphologies of the scaffolds were observable and found to be similar to those of the scaffolds shown in Fig. 7a, e, and i. Interconnected pore structures were visible in each scaffold. As shown in Fig. 7c, g, and k, the general morphology and interconnected pore structure of each scaffold was observable at the microscopic level.

As shown in Fig. 7d, h, and l, the formation of HA on the surface of each scaffold was visible, with more and better ordered HA on the surfaces of MBG and MBG–HACC scaffolds than on MBG–HACC–Zein scaffolds. This is because HACC is readily water soluble and can dissolve in SBF quickly without having any significant impact on the growth of HA on the surface of the scaffold, but Zein dissolves slowly, and undissolved Zein on the surface of the scaffold hinders the growth and arrangement of HA.

3.2.5 Mechanical properties. As shown in Fig. 8, the compressive strength of pure MBG, MBG–HACC, and MBG–HACC–Zein scaffolds were 59.6 kPa, 200.3 kPa, and 323.3 kPa. After soaking in SBF at a temperature of 37 °C for 24 h, the compressive strengths of pure MBG, MBG–HACC, and MBG–HACC–Zein scaffolds were 57.4 kPa, 76.3 kPa, and 285.1 kPa.

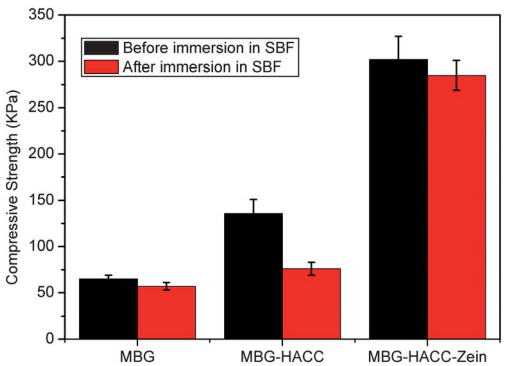

Fig. 8 Mechanical properties of MBG, MBG–HACC, and MBG–HACC–Zein scaffolds before and after soaking in SBF for 1 day.

According to these data, HACC and Zein modifications significantly improved the mechanical strength of MBG scaffolds in the dry state. After soaking in SBF, the mechanical strength of the MBG–HACC scaffolds decreased significantly, and the strength of the MBG–HACC–Zein scaffolds decreased slightly. This was because water-soluble HACC was gradually released from the MBG–HACC scaffolds during soaking. This caused a significant decrease in the mechanical strength of the MBG–HACC scaffolds, and the Zein coating prevented the release of HACC, maintaining the mechanical strength of the MBG–HACC–Zein scaffolds.

3.2.6 SRμCT. SRμCT imaging showed the average sizes of the pores in the MBG–HACC–Zein scaffolds to be about 200 μm. As shown in Fig. 9, the synthesized MBG–HACC–Zein scaffold had a structure including well-interconnected pore channels. These channels facilitate cell ingrowth and the transportation of nutrients, leading to better bone healing.[41]

3.3 Antibacterial efficacy of different scaffolds

The antibacterial effects of MBG–HACC, MBG–HACC–Zein, HACC, and HACC–Zein were significantly more pronounced than those of MBG after 24 h for ATCC35984 ($P < 0.01$, Fig. 10), and no significant difference was observed among MBG–HACC, MBG–HACC–Zein, HACC, and HACC–Zein after 24 h for ATCC35984 ($P > 0.05$). However, after 72 h for ATCC35984, the antibacterial effects of MBG–HACC–Zein and HACC–Zein were significantly more pronounced than those of MBG, MBG–HACC, and HACC ($P < 0.01$, Fig. 10). For ATCC35984, no significant differences were observed among MBG, MBG–HACC, and HACC at 72 h ($P > 0.05$) or between MBG–HACC–Zein and HACC–Zein ($P > 0.05$). *Escherichia coli* showed results similar to those of ATCC35984 (data not shown).

In these assays, MBG exhibited barely any antibacterial activity. Although the antibacterial activity of MBG–HACC and HACC was equivalent to that of MBG–HACC–Zein and HACC–Zein after 24 h, it was significantly reduced after 72 h, at which time MBG–HACC and HACC had no effective antibacterial action, like MBG. However, the antibacterial activity of MBG–HACC–Zein and HACC–Zein remained very high after both 24 h and 72 h. This clearly indicates that although HACC can significantly improve the antibacterial activity of MBG, this antibacterial effect does not last long. However, Zein protein was associated with long-lasting antibacterial activity.

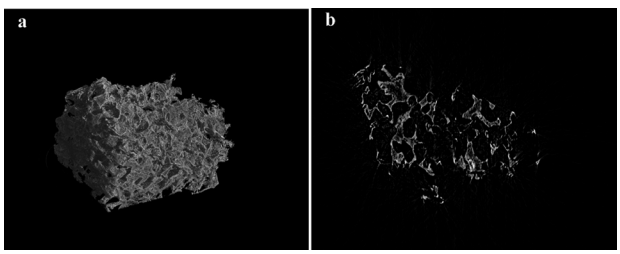

Fig. 9 Macroporous network and strut microstructure of MBG–HACC–Zein scaffolds as shown using SRμCT.

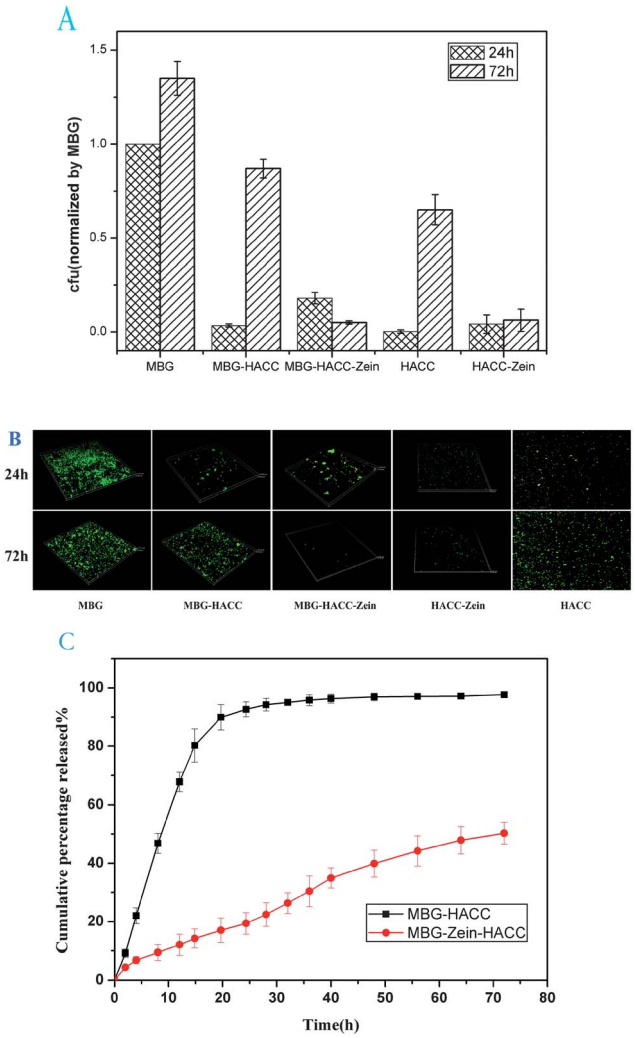

Fig. 10 (A) After 24 h, the antibacterial effects of MBG–HACC, MBG–HACC–Zein, HACC and HACC–Zein were significantly higher than those of MBG ($P < 0.01$), and no significant differences were observed among MBG–HACC, MBG–HACC–Zein, HACC, and HACC–Zein scaffolds ($P > 0.05$). After 72 h, the antibacterial effects of MBG–HACC–Zein and HACC–Zein were significantly higher than those of MBG, MBG–HACC, and HACC ($P < 0.01$), and no significant differences were observed among MBG, MBG–HACC, and HACC ($P > 0.05$) or between MBG–HACC–Zein and HACC–Zein ($P > 0.05$). (B) Projected top views of antibacterial efficacy of different scaffolds against ATTCC35984 after 24 h and 72 h. Images were obtained using confocal laser scanning microscopy (CLSM) after staining with the Baclight dead/live stain. Bacteria were stained with green fluorescent SYTO 9 and red fluorescent propidium iodide, which causes live cells to appear green and dead cells to appear red under CLSM. Magnification, ×400. (C) HACC cumulative relative release profiles from HACC- and HACC–Zein-modified MBG scaffolds soaked in SBF for 72 h.

3.4 Biocompatibility of different scaffolds

The viability of hMSCs on the scaffolds was visualized using a fluorescent live/dead assay. Live hMSCs were stained green and appeared to have adhered to the scaffolds, and dead cells were stained red. The cell status 24 h after seeding on three kinds of scaffolds is shown in Fig. 11. A few dead cells (red spots) were observed on the MBG–HACC scaffold, which indicated that, after 24 h, there were several dead cells with damaged membranes. Few dead cells were visible on the MBG and

MBG–HACC–Zein scaffolds. The relative number of live cells was not significantly different among MBG, MBG–HACC, and MBG–HACC–Zein scaffolds ($P > 0.05$).

3.5 Cell proliferation

The cell proliferation data collected from the samples after 4 and 7 days were normalized to data collected on day 1. Cells on the MBG scaffold showed a proliferation rate notably higher than those of cells on other scaffolds at all points in time (Fig. 12). On day 4, the cells on the MBG–HACC, MBG–HACC–Zein, HACC, and HACC–Zein scaffolds showed lower proliferation rates than those on the MBG scaffold (Fig. 12). On day 7, the proliferation rate of the cells on the MBG scaffold became significantly higher than those of cells on the MBG–HACC, MBG–HACC–Zein, HACC, or HACC–Zein scaffolds (Fig. 12). The relative proliferation rate of the hMSCs on the MBG, MBG–HACC, MBG–HACC–Zein, HACC, and HACC–Zein scaffolds tended to increase from day 1 to day 7. However, the proliferation rate of cells on the MBG–HACC and HACC scaffolds tended to decrease from day 4 to day 7 (Fig. 12).

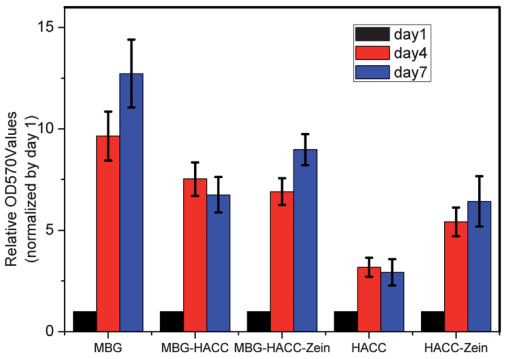

Fig. 12 Proliferation of hMSCs on the MBG, MBG–HACC, MBG–HACC–Zein, HACC, and HACC–Zein scaffolds.

4 Discussion

In the present study, we analyzed the effects of HACC and HACC–Zein on the physical and chemical properties, antibacterial activity, and biological features of MBG scaffolds. The results showed that both HACC and HACC–Zein could improve the mechanical strength of MBG, which was brittle and had many unconnected pore walls.[8] Surface modifications involving HACC were found to improve the mechanical properties of MBG. Its compressive strength increased from 59.6 kPa to 200.3 kPa. The pore walls of MBG remained well connected. The HACC–Zein modified MBG was characterized by further improvement of the glass's mechanical properties. Compressive strength increased to 323.3 kPa, five times the original value. Ductility was further enhanced in this way. The connected pore structure of the HACC–Zein-modified MBG scaffold remained well preserved.

Unmodified MBG has no antibacterial activity. The present study showed large numbers of bacteria on the surface of the MBG after both 24 h and 72 h. The HACC-modified MBG scaffold showed strong antibacterial activity after 24 h, and the number of bacteria had increased by 72 h, which indicates that HACC-modified MBG lacks long-term antibacterial activity. HACC–Zein-modified MBG scaffolds were characterized by low levels of bacteria on the surface after both 24 h and 72 h, which demonstrates that it possesses both short-term and long-term antibacterial activities. This is because HACC is water-soluble and Zein is not.[32] During the degradation of the scaffold, Zein can slow the release of HACC, resulting in prolonged antibacterial action. In order to prove this, we plotted a curve of the gradual release of HACC from MBG–HACC and MBG–HACC–Zein scaffolds incubated in SBF for 72 h. The results showed that HACC was almost completely released from the MBG–HACC scaffolds within 12 h of soaking, and the release of HACC from the MBG–Zein–HACC scaffolds took place significantly more slowly, where only 50.3% of HACC had been released after 72 h of soaking. This was because of the protection offered by the Zein coating, which prolonged the antibacterial effects of the MBG–HACC–Zein scaffolds (Fig. 10C). The FT-IR and TGA results of the MBG–HACC scaffolds soaked in SBF for 72 h were found to be consistent with this point (ESI Fig. S3 and S4†).

Calcium phosphate formed on the surfaces of both HACC-modified MBG and HACC–Zein-modified-MBG scaffolds after immersion in SBF, which indicates that both were highly bioactive. Cells also grew well on their surfaces. However, the cell proliferation rate for HACC-modified MBG was slow at 7 days. This might have been due to inhibition by HACC. The confocal image taken at this point in time also showed some dead cells. The cells on the surfaces of the HACC–Zein-modified MBG scaffolds showed higher proliferation rates than those on the surfaces of the HACC-modified-MBG scaffolds. There were also fewer dead cells on the HACC–Zein-modified MBG scaffolds at these points in time.

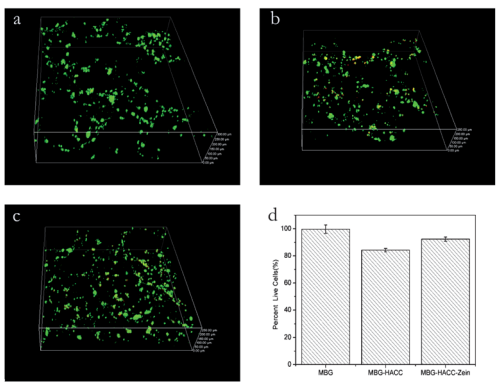

Fig. 11 Fluorescence photographs of hMSC proliferation on (a) MBG, (b) MBG–HACC, and (c) MBG–HACC–Zein after 24 h. (d) Relative number of live cells.

5 Conclusion

In this study, meso-macroporous MBG scaffolds, both HACC-coated and HACC–Zein-coated, were all successfully prepared. Surface modification with HACC or HACC–Zein was found to improve the mechanical properties of the MBG scaffolds.

Mesoporous bioglass (MBG) was not found to have any antibacterial activity, and MBG modified with HACC showed only short-term antibacterial activity, but MBG modified with HACC–Zein showed both short-term and long-term antibacterial activity. Human mesenchymal stem cells (hMSCs) were found to adhere to the pore walls of all three types of scaffolds. Some dead cells were observed on the HACC-modified MBG scaffolds. There were fewer dead cells on the HACC–Zein-modified MBG scaffolds. HACC–Zein-modified MBG shows significant promise as a material for use in bone repair in that it has an interconnected pore structure, good mechanical strength, minimal susceptibility to degradation, and long-lasting antibacterial activity.

Acknowledgements

This work received support from the Nano Project of Science and Technology Commission of Shanghai Municipality (no. 1052nm03100), Key Projects for Basic Research Shanghai Committee of Science and Technology (no. 11JC1415700), and National Natural Science Foundation of China (no. 81171794).

Notes and references

1 F. J. O'Brien, *Mater. Today*, 2011, **14**, 88–95.
2 F. M. Chen, R. Chen, X. J. Wang, H. H. Sun and Z. F. Wu, *Biomaterials*, 2009, **30**, 5215–5224.
3 B. Duan, M. Wang, W. Y. Zhou, W. L. Cheung, Z. Y. Li and W. W. Lu, *Acta Biomater.*, 2010, **6**, 4495–4505.
4 Y. B. Kim and G. H. Kim, *J. Mater. Chem.*, 2012, **22**, 16880–16889.
5 X. X. Yan, C. Z. Yu, X. F. Zhou, J. W. Tang and D. Y. Zhao, *Angew. Chem., Int. Ed.*, 2004, **43**, 5980–5984.
6 L. L. Hench, R. J. Splinter, T. K. Greenlee and W. C. Allen, *J. Biomed. Mater. Res.*, 1971, **2**, 117–141.
7 X. X. Yan, X. H. Huang, C. Z. Yu, H. X. Deng, Y. Wang and Z. D. Zhang, *et al.*, *Biomaterials*, 2006, **27**, 3396–3403.
8 C. T. Wu, Y. X. Luo, G. Cuniberti, Y. Xiao and M. Gelinsky, *Acta Biomater.*, 2011, **7**, 2644–2650.
9 Y. F. Zhu, C. T. Wu, Y. Ramaswamy, E. Kockrick, P. Simon and S. Kaskel, *et al.*, *Microporous Mesoporous Mater.*, 2008, **112**, 494–503.
10 C. T. Wu, Y. H. Zhou, W. Fan, P. P. Han, J. Chang and J. Yuen, *et al.*, *Biomaterials*, 2012, **33**, 2076–2085.
11 T. A. Ostomel, Q. H. Shi, C. K. Tsung, H. J. Lang and G. D. Stucky, *Small*, 2006, **2**, 1261–1265.
12 W. Xia and J. Chang, *J. Controlled Release*, 2006, **110**, 522–530.
13 C. T. Wu, Y. F. Zhang, Y. F. Zhu, T. Friis and Y. Xiao, *Biomaterials*, 2010, **31**, 3429–3438.
14 W. Zimmerli, A. Trampuz and P. E. Ochsner, *N. Engl. J. Med.*, 2004, **351**, 1645–1654.
15 T. Berendt and I. Byren, *Clin. Med.*, 2004, **4**, 510–518.
16 M. A. Cataldo, N. Petrosillo, M. Cipriani, R. Cauda and E. Tacconelli, *J. Infect.*, 2010, **61**, 443–448.
17 M. J. Enzler, E. Berbari and D. R. Osmon, *Mayo Clin. Proc.*, 2011, **86**, 686–701.
18 D. Campoccia, L. Montanaro, P. Speziale and C. R. Arciola, *Biomaterials*, 2010, **31**, 6363–6377.
19 J. P. Steinberg, B. I. Braun, W. C. Hellinger, L. Kusek, M. R. Bozikis and A. J. Bush, *et al.*, *Ann. Surg.*, 2009, **250**, 10–16.
20 J. C. Martínez-Pastor, F. Vilchez, C. Pitart, J. M. Sierra and A. Soriano, *Eur. J. Clin. Microbiol. Infect. Dis.*, 2010, **29**, 1039–1041.
21 L. R. Martinez, M. R. Mihu, M. Tar, R. J. Cordero, G. Han and A. J. Friedman, *et al.*, *J. Infect. Dis.*, 2010, **201**, 1436–1440.
22 E. M. Costa, S. Silva, C. Pina, F. K. Tavaria and M. M. Pintado, *Anaerobe*, 2012, **18**, 305–309.
23 S. Y. Ong, J. Wu, S. M. Moochhala, M. H. Tan and J. Lu, *Biomaterials*, 2008, **29**, 4323–4332.
24 M. Kong, X. G. Chen, K. Xing and H. J. Park, *Int. J. Food Microbiol.*, 2010, **144**, 51–63.
25 L. Wang and J. P. Stegemann, *Biomaterials*, 2010, **31**, 3976–3985.
26 N. Bhardwaj, Q. T. Nguyen, A. C. Chen, D. L. Kaplan, R. L. Sah and S. C. Kundu, *et al.*, *Biomaterials*, 2011, **32**, 5773–5781.
27 P. K. Dutta, J. Dutta and V. S. Tripathi, *J. Sci. Ind. Res.*, 2004, **63**, 20–31.
28 Z. X. Peng, L. Wang, L. Du, S. R. Guo, X. Q. Wang and T. T. Tang, *Carbohydr. Polym.*, 2010, **81**, 275–283.
29 H. L. Tan, Z. X. Peng, Q. T. Li, X. F. Xu, S. R. Guo and T. T. Tang, *Biomaterials*, 2012, **33**, 365–377.
30 T. Y. Wu, X. L. Hua, Z. W. He, X. F. Wang, X. W. Yu and W. P. Ren, *Biomed. Mater.*, 2012, **7**, 045003.
31 H. J. Wang, Z. X. Lin, X. M. Liu, S. Y. Sheng and J. Y. Wang, *J. Controlled Release*, 2005, **105**, 120–131.
32 X. N. Li, H. X. Guo and J. Heinamaki, *J. Colloid Interface Sci.*, 2010, **345**, 46–53.
33 S. Subramanian and S. Sampath, *Biomacromolecules*, 2007, **8**, 2120–2128.
34 Z. B. Gao, P. T. Ding, L. Zhang, J. Shi, S. Q. Yuan and J. Wei, *et al.*, *Int. J. Pharm.*, 2007, **328**, 57–64.
35 J. Bai, V. Alleyne, R. D. Hagenmaier, J. P. Mattheis and E. A. Baldwin, *Postharvest Biol. Technol.*, 2003, **28**, 259–268.
36 A. C. S. Alcântara, P. Aranda, M. Darder and E. Ruiz-Hitzky, *J. Mater. Chem.*, 2010, **20**, 9495–9504.
37 L. Liu, M. L. Fishman, K. B. Hicks, M. Kende and G. Ruthel, *Drug Delivery*, 2006, **13**, 417–423.
38 T. M. Auschill, N. Hein, E. Hellwig, M. Follo, A. Sculean and N. B. Arweiler, *J. Clin. Periodontol.*, 2005, **32**, 147–152.
39 J. LÖnn-Stensrud, M. A. Landin, T. Benneche, F. C. Petersen and A. A. Scheie, *J. Antimicrob. Chemother.*, 2009, **63**, 309–316.
40 L. D. Warren, A. E. Clark and L. L. Hench, *J. Biomed. Mater. Res.*, 1989, **23**, 201–209.
41 L. Moroni and J. H. Elisseeff, *Mater. Today*, 2008, **11**, 44–51.

